Peer-reviewed version available at Materials 2019, 12, 965; doi:10.3390/ma12060965

Article

Influence of the loading speed on the ductility properties of corroded reinforcing bars in concrete

Angela M. Bazán[1], M. Nieves González[2], Marcos G. Alberti[1], Jaime C. Gálvez[1*]

[1] Departamento de Ingeniería Civil: Construcción. E.T.S de Ingenieros de Caminos. Canales y Puertos. Universidad Politécnica de Madrid. C / Profesor Aranguren. s/n. 28040. Madrid; angela.moreno@upm.es

[2] Departamento de Tecnología de la Edificación. E.T.S de Edificación. Universidad Politécnica de Madrid Avda. Juan de Herrera. 6. 28040. Madrid. Alfonso.cobo@upm.es

* Correspondence: Jaime.galvez@upm.es; Tel.: +34 910 674125

Abstract: In this work 144 reinforcing bars of high-ductility steel named B500SD were subjected to an accelerated corrosion treatment and then tested under tension at different loading speeds in order to assess the effect of corrosion on the ductility properties of the rebars. Results showed that the bars with a corrosion level as low as the one reducing the steel mass by 1% gave rise to a significant degradation on the ductility properties with strain-stress curves losing the yield plateau and behaving practically as cold deformed steel bars. This effect took place at every tested loading speed. Thus, the research significance relies on the assessment of the influence of the loading speed at which the tensile test is performed given that it affects the ductility properties of the reinforcement bars.

Keywords: Corrosion; Ductility; Mechanical properties; Reinforced concrete; Tensile strength; Equivalent steel.

1. Introduction

The Spanish Structural Concrete Code EHE-08 and the Eurocode EC-2 [1-2] require limited values in the mechanical properties of high-ductility steel in terms of both strength and strain. The rebar strength has a significant influence on the structural strength of concrete reinforced members and the codes require minimum values for the steel yield strength and maximum tensile strength. Additionally, due to the consideration of dynamic and seismic actions, it is also required to consider properties in relation to the steel ductility. One way in which ductility can be considered is in relationship with the fracture energy that is the area covered by the strain-stress curve. This energy depends on the plastic deformation capacity of steel up to the breaking point. The higher the area, the higher is the capacity of steel to dissipate energy under dynamic loads. Also, for dynamic and impact loads it is important the speed at which the load is applied.

In reinforced concrete members, the concrete cover provides protection to the rebars both physical and chemical. The alkaline environment of concrete [3-4] protects the rebars against the corrosion. In these conditions, the presence of enough humidity triggers the steel corrosion process. Three consequences take place when the steel bars start corroding: i) loss of steel material converted in rust reducing the bar section area and the ductility [5-8] ii) cracking and spalling of the concrete cover and iii) loss of bonding between concrete and steel bar that reduces the efficiency of the reinforced concrete system [9-10].

The Codes EHE-08 and EC-2 require that the steel bars meet ductility properties based on maximum strain (ε_{max}) and the ratio between maximum strength and the elastic limit (f_s/f_y). Table 1 shows the limits of those parameters as required by the EHE-08 code in order to qualify the steel as

Peer-reviewed version available at Materials 2019, 12, 965; doi:10.3390/ma12060965

of high ductility according to standard UNE 36065:2011 [11]. Also, the average strain value assessed over a length of 5 bar diameters (ε5Ø) is included in this code although is not considered in other codes.

Table 1. Requirements of the EHE-08 code for B500SD steel.

fy	**f_s**	**f_s/f_y**	**εmax**	**ε5ϕ**
500 MPa	575 MPa	$1.15 \leq f_s/f_y \leq 1.35$	≥7.5%	≥16%

The classical approach to steel rebar corrosion considers a reduction in the area of the bar section proportional to the degree of corrosion. Most of the works [12-14] report systematic reduction of strength and strain at maximum load when the degree of corrosion increases. If this occurs in a constant homogeneous trend. The loss of strength becomes proportional to the loss of bar section area. Recent studies [15- 16] have demonstrated that the corrosion takes place in local spots of the bar surface (pitting), a weakening of strength occurs at these spots (notch effect), and the bar strength falls under the minimum values required by the codes, even with very small degrees of corrosion. Nevertheless, the reduction of strain is greater than the loss of strength in the bar.

With low levels of corrosion, the loss of strength is also low, and the structural elements can still meet their resistance function, but the reduction of strain may not meet the minimum values required in Table 1 to ensure enough ductility. Previous studies [17] show that the ratio *fs/fy* remains constant with the increase of the corrosion level. That means that the steel may amply meet the *fs/fy* requirement but not the requirement of ε_{max}.

In these cases, the use of "equivalent steel" concept as a ductility criterion based on both *fs/fy* and ε_{max} can be very useful. Table 2 shows the minimum values obtained with the EHE-08 requirements in application of the equivalent steel formulas [18-23] as proposed by Cosenza (*p*), Creazza (*A**) and Ortega (*Id*).

Table 2. Values of the equivalent steel parameters obtained with EHE-08 high ductility steel requirements.

	Cosenza (*ρ*)	**Creazza (*A**)**	**Ortega (*Id*)**
Normative EHE-08	0.82	3.87	63.65

In this work the variations of the mechanical steel properties as a function of the degree of corrosion and of the increasing speed of the applied load are reported. For that purpose, 144 bars of 12 mm diameter of reinforcing high ductility steel, named B500SD, were tested in tension after an accelerated corrosion treatment when embedded in NaCl contaminated concrete.

2. Materials and Methods

2.1 Materials

Twelve concrete slabs of 30x40x10 cm^3 were fabricated each one with 12 reinforcing bars partially embedded, making a total of 144 bars to be corroded and tested in tension (Figure 1). The steel type was B500SD used normally in structures in seismic areas due to the higher properties in terms of ductility.

Peer-reviewed version available at Materials 2019, 12, 965; doi:10.3390/ma12060965

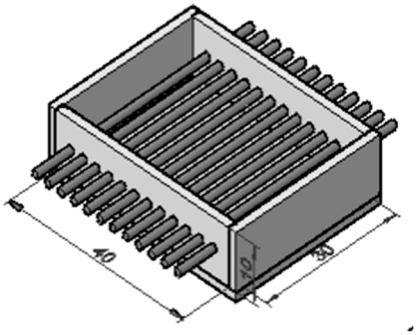

Figure 1. Cats used for the fabrication of slabs (30x40x10 cm³)

River silica, san, round gravel and cement CEM II/A-L 32.5, according to standard RC-16 [24] were the mix basic materials. NaCl with a concentration of 2% relative to the weight of cement was diluted in the mixing tap water in order to destroy the passive state of the reinforcing bars. After casting and demolding the slabs were cured for 28 days in chamber under ambient conditions control at 25ºC and 99% relative humidity. In order to avoid corrosion initiation and propagation at the point, where the bars protrude the concrete slab each bar was wrapped with insulating tape in these points for 3 cm lengths outside and inside of concrete.

2.2 Accelerated corrosion

The accelerated corrosion process was activated by using an electrical current concrete-steel and the application of a constant anodic current between the bars and a lead plate placed on top of the slabs, acting as the cathode. A soaked textile pad placed in between the concrete slab and the lead plate ensured the even distribution of the electric current.

The value of the current in each bar was controlled by means of a digital multimeter. reading periodically the voltage and adjusting the electrical potential at the power source to ensure a constant current value of approximately 10μA/cm² in each bar. In order to achieve different corrosion levels, the current was disconnected at different ages after cracks appeared in the concrete slabs (Figure 2). Once the corrosion process was over, the slabs were demolished, and the oxide of each bar surface was eliminated using a brush according to standard ASTM G 190-06 [25] followed by a chemical pickling according to standard ISO 8407 [26].

The corrosion level of each bar was quantified by a variable *Qmax* assessed by gravimetric procedures. weighing the bars after the full cleaning of all corrosion products and assuming that the loss of steel has been uniform in the corroded bar length Lc that is the equation:

$$Q_{corr} = \frac{100(Pi-Pc)}{Pi}, \quad (1)$$

Where Q_{corr} is the percentage of weight loss and *Pi* and *Pc* are the initial (previous to the slab fabrication) and final weight of the bar, respectively.

Peer-reviewed version available at Materials 2019, 12, 965; doi:10.3390/ma12060965

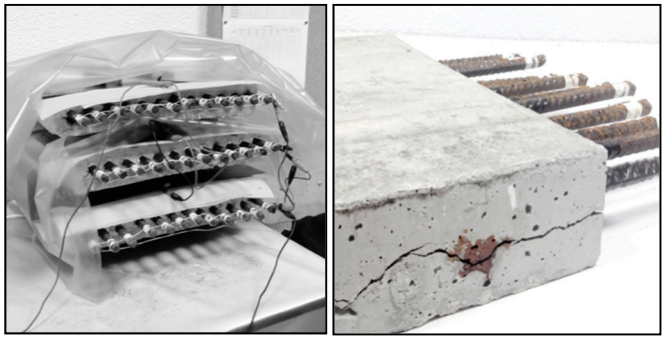

Figure 2. Electrical connection of the bars for the accelerated corrosion process (left hand side) and cracks in the concrete slabs after disconnecting and ready for demolition (right hand side).

The residual value of the bar cross-section area as average in the length *Lc* can be determined by the equation:

$$S_{res} = \frac{Pc}{7.85\ Lc} \quad (2)$$

Where S_{res} is the equivalent residual section (cm^2), *Lc* is the corroded length of the bar (cm) and 7.85 is the specific weight of steel (g/cm^3).

2.3 Strength tests

Once the corrosion process was finished and the bars free of all corrosion products, bars were tested in tension according to standard EN ISO 6982-1:2009 [40] by a multitest IBERTEST press with a loading capacity of 100 kN, controlled by WINTest 32 software program. The strain measurements were performed with an extensometer 2-IBER-25 with 50 mm base.

Before the test, each bar was painted in its length with lines separated by one centimeter in order to measure the ultimate strain after the test as can be seen in Equations 3 and 4. The $\epsilon_{5\phi}$ is the strain after failure and it is assessed including the necking. The ϵ_{max} is the strain under maximum load and it is assessed before the formation of the necking.

$$\varepsilon_{5\phi} = \frac{d - d_0}{d_0} \times 100 \quad (3)$$

$$\varepsilon_{max} = \frac{d - d_1}{d_1} \times 100 \quad (4)$$

The development of the tests was controlled in terms of load when the bar behaved in the elastic range and in terms of deformation when the test was running in the plastic zone by three different speeds. The standard speed Vm was the one recommended by standard UNE-EN ISO 15630-1: 2011 [27] that is 3.7 kNs and 20.1 mm/min. A speed three times faster Vh with 11.1 kN/s and 60.3 mm/m and a speed Vl three times slower with 1.23 kN/s and 6.7 mm/min were also used.

A designating code B-XXX-Y was used to identify each bar sample, B meaning "bar", XX the bar number (1 to 144) and Y the loading speed (Low, Medium or High). The (*) in the nomenclature shows that the rebar does not meet some of the EHE-08 requirements for B500SD steel.

3. Results

Preprints (www.preprints.org) | NOT PEER-REVIEWED | Posted: 28 January 2019 doi:10.20944/preprints201901.0279.v1

Peer-reviewed version available at Materials 2019, 12, 965; doi:10.3390/ma12060965

Based on the test results, the values of the equivalent steel ductility parameters as per Ortega (*Id*), Cosenza (*p*) and Creazza (*A**) were calculated for each bar sample. Tables 3, 4 and 5 show the results and the ductility parameters for low, medium and high loading speed, respectively. The level of corrosion has been quantified by Q_{corr} as per Equation 1 and has been used to put in order the Table lists. Results include the elastic limit (*fy*), maximum unit tension load (*fs*), the strain at maximum load ε_{max} and the maximum strain obtained over a five-diameter length $\varepsilon_{5}\emptyset$. All mechanical properties were calculated with respect to the residual equivalent cross section area S_{res} (Equation 2). Also, the equivalent steel ductility parameters were calculated with respect Equation 5, 6 and 7.

$$\mathrm{Id} = 1 + \left(1 + \frac{fs}{fy}\right)\left(\frac{\varepsilon\, max}{\varepsilon\, y} - 1\right), \tag{5}$$

$$\mathrm{A^*} = \frac{2}{3}(fs - fy)(\varepsilon\, max\ - \varepsilon\, sh), \tag{6}$$

$$\mathrm{P} \approx\ \varepsilon max^{0.75}\left(\frac{fs}{fy} - 1\right)^{0.9}, \tag{7}$$

Those bars with lower values of any of the mechanical parameters than those required for steel B500SD in EHE-08 have been highlighted with an asterisk in Table 3, Table 4 and Table 5.

Table 3. Results of tensile tests on 12 mm diameter bars with increasing corrosion rates (Q_{corr}) using load increment speed (Vl) of 1.23 kN/s up to the elastic limit (*fy*) and a deformation speed of 6.7 mm/min the plastic zone. The three values of equivalent steel criteria for each bar have also been included.

Rebars	Loading speed	Q_{corr} (%)	*fy* (MPa)	*fs* (MPa)	*fs*/*fy*	ε_{max} (%)	$\varepsilon_{5\emptyset}$ (%)	*Id*	*P*	*A** (N/mm²)
B001L	1.23	0.00	534.02	614.83	1.15	17.11	27.00	135.10	1.53	9.51
B002L	1.23	0.00	529.28	610.33	1.15	16.19	27.00	127.77	1.46	9.03
B003L	1.23	0.03	526.54	603.69	1.15	13.89	25.00	118.30	1.30	7.37
B004L	1.23	0.06	526.99	612.10	1.16	15.55	30.00	110.80	1.50	9.11
B005L	1.23	0.08	526.89	606.71	1.15	14.06	28.00	106.81	1.32	7.72
B006L	1.23	0.10	529.58	609.96	1.15	15.24	27.00	120.21	1.40	8.43
B007L	1.23	0.15	535.34	612.49	1.15	13.17	28.00	99.98	1.25	6.99
B008L	1.23	0.19	526.24	607.37	1.15	13.40	28.00	101.74	1.27	7.48
B009L	1.23	0.23	537.76	612.43	1.15	11.49	28.00	87.08	1.13	5.90
B010L*	1.23	0.34	527.42	566.81	1.07	8.15	26.00	63.82	0.44	2.21
B011L	1.23	0.34	500.29	592.84	1.18	11.43	28.00	87.81	1.33	7.28
B012L	1.23	0.37	523.30	609.90	1.17	17.29	28.00	132.83	1.72	10.30
B014L	1.23	0.44	530.93	613.33	1.16	16.41	29.00	121.07	1.57	9.30
B015L	1.23	0.44	508.94	587.13	1.15	10.70	26.00	87.33	1.07	5.76
B016L	1.23	0.49	520.56	602.64	1.16	12.27	28.00	93.49	1.26	6.93
B017L	1.23	0.50	534.85	615.64	1.15	15.63	-	-	1.43	8.69
B018L	1.23	0.52	530.37	616.35	1.16	12.64	28.00	96.35	1.29	7.48
B019L	1.23	0.53	530.37	616.35	1.16	12.64	28.00	96.35	1.29	7.48
B020L	1.23	0.68	533.98	612.36	1.15	12.87	26.00	105.28	1.23	6.94
B021L	1.23	0.70	524.22	608.98	1.16	14.94	28.00	114.09	1.46	8.71
B022L	1.23	0.76	516.12	601.71	1.17	13.51	30.00	96.55	1.43	7.96
B023L	1.23	0.80	520.95	601.50	1.15	11.34	27.00	89.15	1.12	6.28
B024L*	1.23	0.82	475.96	545.98	1.15	8.93	34.00	55.32	0.94	4.30
B025L	1.23	0.84	536.17	617.64	1.15	12.13	30.00	85.78	1.18	6.80

Preprints (www.preprints.org) | NOT PEER-REVIEWED | Posted: 28 January 2019 doi:10.20944/preprints201901.0279.v1

Peer-reviewed version available at Materials 2019, 12, 965; doi:10.3390/ma12060965

B026L	1.23	0.89	504.97	589.03	1.17	9.88	28.00	75.40	1.13	5.71
B027L	1.23	0.94	526.27	605.27	1.15	12.57	24.00	111.46	1.21	6.83
B028L	1.23	1.03	500.76	578.25	1.16	9.54	24.00	84.70	1.04	5.09
B029L*	1.23	1.05	490.76	578.25	1.18	9.54	29.00	70.53	1.16	5.74
B030L*	1.23	1.05	530.38	616.35	1.16	8.05	29.00	58.80	0.92	4.76
B031L*	1.23	1.13	651.71	726.36	1.11	8.64	27.00	66.41	0.69	4.44
B032L	1.23	1.19	506.27	589.77	1.16	11.02	26.00	90.39	1.16	6.33
B033L	1.23	1.21	502.03	585.89	1.17	9.34	28.00	71.22	1.08	5.39
B034L*	1.23	1.30	458.23	548.45	1.20	7.99	28.00	61.58	1.12	4.96
B035L	1.23	1.40	506.27	589.77	1.16	11.02	25.00	94.05	1.16	6.33
B036L	1.23	1.58	501.61	588.23	1.17	8.43	25.00	72.00	1.00	5.02
B037L*	1.23	1.74	479.76	561.71	1.17	7.92	26.00	64.93	0.96	4.47
B038L*	1.23	1.80	485.23	575.16	1.19	9.09	25.00	78.44	1.17	5.62
B039L*	1.23	2.06	470.60	565.26	1.20	8.71	26.00	72.50	1.19	5.67
B040L*	1.23	2.18	493.22	570.42	1.16	8.91	29.00	65.20	0.99	4.73
B041L*	1.23	2.36	470.79	558.30	1.19	7.67	28.00	58.80	1.03	4.62
B042L*	1.23	2.38	462.84	531.12	1.15	6.05	27.00	47.03	0.70	2.84
B043L*	1.23	2.46	478.80	572.32	1.20	9.94	27.00	79.79	1.32	6.40
B044L*	1.23	2.52	471.37	550.49	1.17	8.41	28.00	64.01	1.00	4.58
B045L*	1.23	2.85	460.34	537.38	1.17	6.35	25.00	53.95	0.81	3.37
B046L*	1.23	2.93	458.23	548.45	1.20	8.02	31.00	55.72	1.12	4.98
B047L*	1.23	3.12	429.57	518.82	1.21	14.30	26.00	120.34	1.81	8.78
B048L*	1.23	4.66	458.03	541.86	1.18	6.90	23.00	64.22	0.91	3.98

Table 4. Results of tensile tests on 12 mm diameter bars with increasing corrosion rates (Q_{corr}) using load increment speed (Vm) of 3.7 kN/s up to the elastic limit (fy) and a deformation speed of 20.1 mm/min the plastic zone. The three values of equivalent steel criteria for each bar have also been included.

Rebars	Loading speed	Q_{corr} (%)	fy (MPa)	fs (MPa)	fs/fy	ε_{max} (%)	$\varepsilon_{5\emptyset}$ (%)	Id	P	A^* (N/mm²)
B049M*	3.70	0.00	544.38	626.03	1.15	13.94	25.00	118.73	1.31	7.83
B050M	3.70	0.00	553.64	636.67	1.15	13.05	28.00	99.06	1.25	7.45
B051M	3.70	0.02	521.19	605.10	1.16	14.82	27.00	117.40	1.45	8.56
B052M*	3.70	0.09	538.32	612.13	1.14	14.18	27.00	111.25	1.25	7.20
B053M	3.70	0.11	529.48	608.73	1.15	12.48	31.00	85.40	1.20	6.80
B054M	3.70	0.14	518.72	604.69	1.17	13.14	30.00	93.88	1.40	7.77
B055M*	3.70	0.14	522.14	602.23	1.15	12.05	7.00	368.96	1.17	6.64
B056M	3.70	0.15	522.38	606.17	1.16	12.06	25.00	103.04	1.24	6.95
B057M	3.70	0.15	521.38	597.59	1.15	13.89	19.00	156.03	1.30	7.28
B058M	3.70	0.15	530.81	609.75	1.15	14.49	28.00	110.11	1.35	7.87
B059M	3.70	0.15	531.79	609.79	1.15	13.45	26.00	110.07	1.27	7.22
B060M	3.70	0.15	531.00	611.39	1.15	12.99	27.00	102.29	1.24	7.18
B061M	3.70	0.16	530.90	610.20	1.15	14.02	27.00	110.49	1.31	7.65
B062M	3.70	0.17	529.11	614.76	1.16	13.35	19.00	150.61	1.34	7.87
B063M*	3.70	0.19	541.84	612.54	1.13	14.31	-	-	1.17	6.96
B064M	3.70	0.22	525.96	608.02	1.16	12.79	28.00	97.51	1.30	7.22
B065M	3.70	0.23	515.56	601.22	1.17	13.21	28.00	101.21	1.41	7.79
B066M	3.70	0.26	532.26	612.23	1.15	14.75	28.00	112.11	1.36	8.12
B067M*	3.70	0.27	520.20	586.33	1.13	9.11	25.00	76.49	0.84	4.14
B068M	3.70	0.27	528.04	610.59	1.16	12.73	28.00	97.04	1.30	7.23
B069M	3.70	0.32	526.21	608.61	1.16	14.12	28.00	107.77	1.40	8.00

Preprints (www.preprints.org) | NOT PEER-REVIEWED | Posted: 28 January 2019 doi:10.20944/preprints201901.0279.v1

Peer-reviewed version available at Materials 2019, 12, 965; doi:10.3390/ma12060965

B070M	3.70	0.34	530.45	612.86	1.16	13.60	28.00	103.75	1.36	7.71
B071M	3.70	0.42	505.66	593.07	1.17	10.60	30.00	75.50	1.19	6.37
B072M	3.70	0.53	525.69	611.00	1.16	11.78	19.00	132.76	1.22	6.91
B073M	3.70	0.60	501.54	584.03	1.20	9.29	26.00	77.41	1.25	5.27
B074M	3.70	0.65	524.12	604.00	1.15	11.62	30.00	82.13	1.14	6.39
B075M	3.70	0.68	531.43	611.32	1.15	12.64	29.00	92.56	1.22	6.95
B076M*	3.70	0.69	527.09	613.29	1.16	11.11	9.00	265.48	1.17	6.59
B077M	3.70	0.70	528.74	606.55	1.15	11.18	26.00	91.30	1.11	5.99
B078M	3.70	0.77	514.27	604.54	1.18	12.63	28.00	97.15	1.43	7.84
B079M	3.70	0.80	525.60	606.32	1.15	11.26	27.00	88.51	1.11	6.25
B080M*	3.70	0.83	620.40	689.72	1.11	8.61	25.00	71.56	0.69	4.11
B081M*	3.70	0.85	518.02	600.39	1.16	11.67	10.00	250.91	1.21	6.61
B082M*	3.70	0.86	626.49	688.27	1.10	9.31	24.00	80.36	0.67	3.96
B083M	3.70	0.87	521.07	598.55	1.15	11.40	34.00	70.94	1.13	6.08
B084M	3.70	0.94	521.33	597.96	1.15	11.67	19.00	130.91	1.14	6.15
B085M	3.70	0.99	520.49	607.14	1.17	12.87	22.00	125.78	1.38	7.67
B086M	3.70	1.01	516.76	599.52	1.16	11.41	25.00	97.42	1.19	6.50
B087M*	3.70	1.08	497.26	577.39	1.16	9.55	31.00	65.38	1.04	5.26
B088M	3.70	1.36	525.72	607.42	1.16	13.13	35.00	79.87	1.33	7.38
B089M*	3.70	1.52	493.80	575.99	1.17	9.00	32.00	59.86	1.05	5.09
B090M*	3.70	1.55	488.25	575.28	1.18	8.14	26.00	67.07	1.03	4.87
B091M*	3.70	1.60	490.75	578.97	1.18	10.29	32.00	68.92	1.23	6.25
B092M*	3.70	3.40	449.01	542.67	1.21	7.19	29.00	53.58	1.08	4.63
B093M*	3.70	3.57	459.52	540.64	1.18	6.55	22.00	63.72	0.87	3.66
B094M*	3.70	3.81	482.57	567.84	1.18	7.81	27.00	61.88	1.00	4.58
B095M*	3.70	3.92	485.04	571.67	1.18	9.54	28.00	73.10	1.16	5.69
B096M*	3.70	4.07	449.41	498.42	1.11	3.70	27.00	27.80	0.37	1.25

Table 5. Results of tensile tests on 12 mm diameter bars with increasing corrosion rates (Q_{corr}) using load increment speed (Vh) of 11.1kN/s up to the elastic limit (*fy*) and a deformation speed of 60.3 mm/min the plastic zone. The three values of equivalent steel criteria for each bar have also been included.

Rebars	Loading speed	Q_{corr} (%)	*fy* (MPa)	*fs* (MPa)	*fs*/*fy*	ε max (%)	$\varepsilon_{5\emptyset}$ (%)	*Id*	*P*	*A** (N/mm²)
B097H*	11.1	0.1	547.27	619.76	1.13	14.62	29	106.25	1.19	7.29
B098H*	11.1	0.23	616.51	685.65	1.11	9.69	28	71.91	0.75	4.61
B099H*	11.1	0.3	540.17	613.85	1.14	14.78	24	130.65	1.28	7.49
B100H	11.1	0.53	510.04	594.97	1.17	9.91	29	72.98	1.13	5.79
B101H*	11.1	0.54	610.05	688.88	1.13	9.51	19	105.48	0.86	5.16
B102H*	11.1	0.64	534.57	609.86	1.14	12.41	31	84.53	1.13	6.43
B103H	11.1	0.68	513.14	599.51	1.17	10.77	29	79.42	1.21	6.40
B104H*	11.1	0.7	593.91	653.23	1.1	7.64	26	60.61	0.58	3.12
B105H	11.1	0.79	517.42	603.96	1.17	11.84	27	93.99	1.30	7.05
B106H	11.1	0.81	509.05	587.82	1.15	9.04	25	76.59	0.95	4.90
B107H	11.1	0.85	518.77	600.78	1.16	10.54	27	83.16	1.12	5.95
B108H*	11.1	0.86	478.64	567.93	1.19	8.08	30	57.79	1.08	4.96
B109H	11.1	0.88	526.21	612.61	1.16	13.76	23	128.06	1.37	8.18
B110H	11.1	1.01	506.82	594.51	1.17	10.48	28	80.05	1.18	6.32
B111H	11.1	1.05	519.43	598.94	1.15	10.87	34	67.59	1.09	5.95
B112H	11.1	1.08	501.11	587.48	1.17	9.49	27	75.10	1.10	5.64
B113H	11.1	1.13	510.5	592.25	1.16	10.18	34	63.51	1.10	5.73

Preprints (www.preprints.org) | NOT PEER-REVIEWED | Posted: 28 January 2019 doi:10.20944/preprints201901.0279.v1

Peer-reviewed version available at Materials 2019, 12, 965; doi:10.3390/ma12060965

B114H*	11.1	1.13	206.02	283.55	1.38	9.5	27	82.36	2.27	5.07
B115H	11.1	1.14	501.47	586.46	1.17	10.06	33	64.98	1.15	5.88
B116H	11.1	1.17	505.71	588.83	1.16	9.99	30	70.77	1.08	5.71
B117H*	11.1	1.23	618.59	685.66	1.11	11.03	24	95.86	0.83	5.09
B118H*	11.1	1.23	524.17	602.87	1.15	8.62	26	70.13	0.91	4.67
B119H	11.1	1.3	526.07	611.08	1.16	10.84	26	88.90	1.15	6.34
B120H*	11.1	1.33	490.11	503.35	1.03	26.41	26	205.17	0.50	2.41
B121H*	11.1	1.33	483.85	568.02	1.17	9.42	26	77.45	1.09	5.46
B122H*	11.1	1.33	490.15	579.27	1.18	8.99	25	77.21	1.11	5.51
B123H*	11.1	1.42	476.63	556.05	1.17	8.26	20	88.45	0.99	4.51
B124H	11.1	1.48	511.58	587.61	1.15	10.78	28	81.63	1.08	5.64
B125H*	11.1	1.49	485.18	567.64	1.17	9.1	30	64.65	1.06	5.16
B126H*	11.1	1.73	481.25	561.14	1.17	8.06	29	59.14	0.97	4.43
B127H*	11.1	1.96	469.95	552.83	1.18	9.13	24	81.75	1.12	5.21
B128H*	11.1	1.99	527.06	596.64	1.13	8.61	27	66.79	0.80	4.12
B129H*	11.1	2.02	492.4	571.87	1.16	7.61	24	67.33	0.88	4.16
B130H*	11.1	2.14	471.82	555.3	1.18	8.52	29	62.87	1.07	4.89
B131H*	11.1	2.33	487.94	570.91	1.17	8.66	27	68.43	1.02	4.94
B132H*	11.1	2.44	461.62	551.6	1.19	6.79	-	-	0.94	4.20
B133H*	11.1	2.49	487.02	570.88	1.17	9.31	25	79.64	1.08	5.37
B134H*	11.1	2.74	465.86	552.9	1.19	10.2	29	75.84	1.28	6.11
B135H*	11.1	3.14	468.11	549.96	1.17	9.13	26	75.03	1.07	5.14
B136H*	11.1	3.18	437.8	539.57	1.23	5.19	27	41.64	0.92	3.63
B137H*	11.1	3.37	479.02	558.81	1.17	6.97	33	44.66	0.87	3.83
B138H*	11.1	3.55	456.71	524.63	1.15	5.98	26	48.30	0.69	2.79
B139H*	11.1	3.74	472.56	557.92	1.18	10.44	25	89.86	1.24	6.13
B140H*	11.1	3.77	459.41	546.98	1.19	9.15	27	73.03	1.18	5.51
B141H*	11.1	4.28	451.88	538.98	1.19	9.14	27	72.95	1.18	5.48
B142H*	11.1	4.3	454.59	536.25	1.18	8.14	26	67.07	1.03	4.57
B143H*	11.1	4.68	476.94	557.9	1.17	7.7	25	65.67	0.94	4.29
B144H*	11.1	5.56	419.32	513.58	1.22	6.89	27	55.43	1.09	4.47

The maximum and minimum values for all the parameters can be seen in Table 6.

Table 6 Range of the mechanical and ductility parameters of tensile tests run at three loading speeds Vl, Vm and Vh

Loading speed	Values	*fy* (*fs*) MPa	*fs*/*fy*	ε max (%)	ε5ø (%)	*Id*	*P*	*A** (N/mm²)
Vl	Min.	429.6(518.8)	1.07	6.05	23	47.0	0.4	2.2
	Max.	651.8(726.4)	1.21	17.29	34	135.1	1.8	10.3
Vm	Min.	449.0(498.4)	1.10	3.7	7	27.8	0.4	1.3
	Max.	626.5(620.40)	1.21	14.8	35	369.0	1.5	8.6
Vh	Min.	206.0(283.6)	1.03	5.2	19	41.6	0.5	2.4
	Max.	618.6(688.9)	1.4	26.4	34	205.2	2.3	8.2

4. Discussion

A general overview of the values in Tables 3, 4 and 5 reveals that, regardless of the loading speed considered. the EHE-08 ductility requirements are met by more than 90% of the bar specimens for corrosion rates up to 1% and that only 20% of the specimens meet such requirements when the corrosion rate is higher than 1%. The main reason for that is the systematic reduction of the strain

Preprints (www.preprints.org) | NOT PEER-REVIEWED | Posted: 28 January 2019 doi:10.20944/preprints201901.0279.v1

Peer-reviewed version available at Materials 2019, 12, 965; doi:10.3390/ma12060965

under maximum load (ε_{max}) for increasing corrosion rates [28] down to values that fail the minimum ones required by EHE-08.

In addition, it is worth noting that the value of f_s/f_y fails for one case at low velocity (Q_{corr}=0.34), for five cases at medium velocity (Q_{corr}> 1%) and for nine cases at high velocity (three for Q_{corr} > 1 %). This ductility criterion is not enough sensible and leads to adopt the term "equivalent steel".

Figure 3 shows the comparative at different loading speeds Vl, Vm and Vh, of the bar specimen percentage that meet the EHE-08 minimum values for high-ductility steel and the fulfilment of the three equivalent steel criteria as per Table 2. The following observations apply:

- For the EHE-08 criteria with corrosion rates up to 1% there is a significant difference for high loading speed Vh as compared to low and medium speeds (Vl, Vm), whereas that difference does not exist for corrosion rates higher than 1%.
- For corrosion rates up to 1% all criteria (EHE-08, Cosenza, Creazza and Ortega) is similarly fulfilled for low and medium loading speeds. For high loading speed, the criteria of EHE-08, Cosenza and Creazza are scarcely fulfilled although the fulfillment is frequent for Ortega criterion.
- With corrosion rates higher than 1% the fulfillment of EHE-08 ductility criteria was low, not so low for Cosenza criterion and high for Creazza and Ortega criterion.

In general, the three equivalent steel concept of Cosenza, Creazza and Ortega are very useful criteria for high loading speeds and corrosion rates under 1%: more that 90% of the bar specimens fulfil the ductility criteria and the concept is quite advantageous to assess the structural ductility with corroded reinforcement.

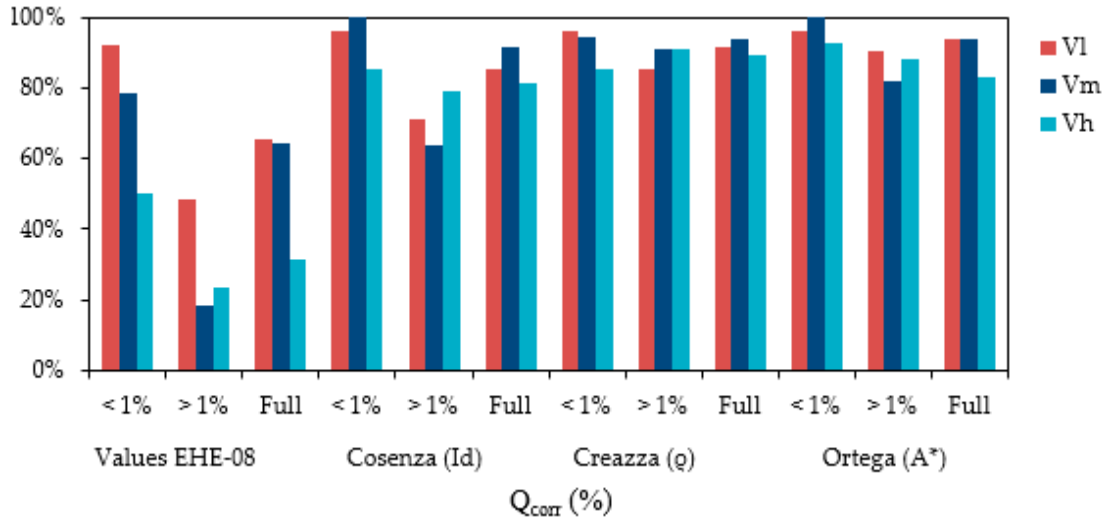

Figure 3. Comparison of the percentage of bar specimens that fulfill different ductility criteria in tensile strength tests run at different loading speeds: low Vl. medium Vm and high Vh.

Summaries of representative strain-stress curves are plotted in Figures 4, 5 and 6 for each loading speed low, medium and high, respectively. It can be seen in all of them that strains at the elastic limit and at the maximum load (ε_{max}) decrease when the corrosion rate increases. This effect is more pronounced for ε_{max}.

If Figure 6 is compared with Figures 4 and 5 it can be observed that the strain in the yield plateau (after the elastic limit is reached) is higher in bar specimens tested at high loading speed as compared with the specimens tested at low and medium loading speeds.

Preprints (www.preprints.org) | NOT PEER-REVIEWED | Posted: 28 January 2019 doi:10.20944/preprints201901.0279.v1

Peer-reviewed version available at Materials 2019, 12, 965; doi:10.3390/ma12060965

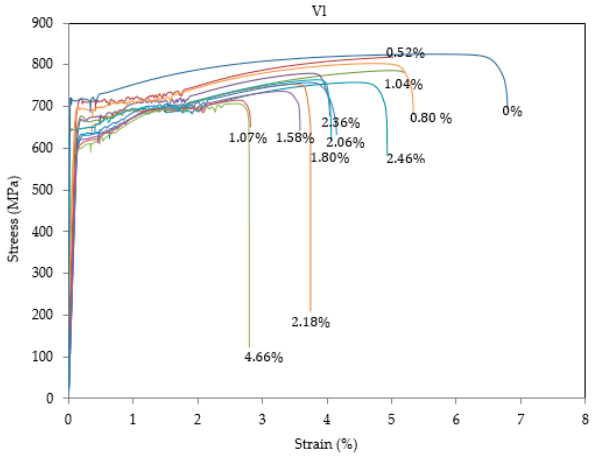

Figure 4. Representative summary of the strain-stress curves of the 48 bar specimens tested at low speed Vl for increasing corrosion rates.

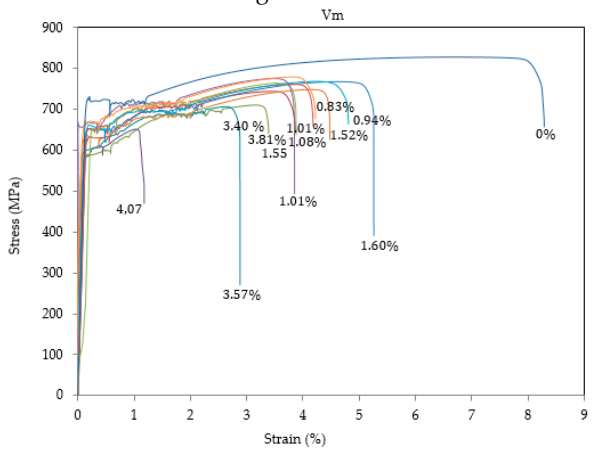

Figure 5. Representative summary of the strain-stress curves of the 48 bar specimens tested at medium (standard) speed Vm for increasing corrosion rates.

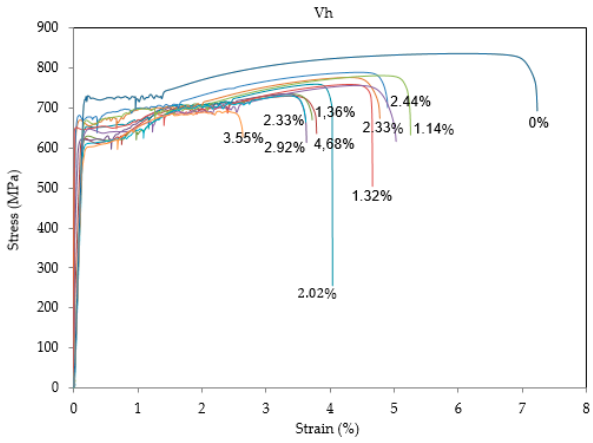

Figure 6. Representative summary of the strain-stress curves of the 48 bar specimens tested at high speed Vh for increasing corrosion rates.

In Figure 7 the total deformation of the bars in the yield zone is plotted for the three loading speeds as a function of the corrosion rate Q_{corr}. It can be observed that the deformation increases when the loading speed increases.

Preprints (www.preprints.org) | NOT PEER-REVIEWED | Posted: 28 January 2019 doi:10.20944/preprints201901.0279.v1

Peer-reviewed version available at Materials 2019, 12, 965; doi:10.3390/ma12060965

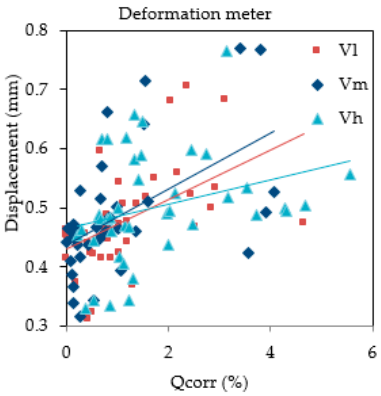

Figure 7. Deformation of bar specimens in the yield zone as a function of the corrosion rate for each of the three loading speeds.

Figure 8 shows the range of the bar deformations in the yield zone for corrosion rates lower than 1% (left) and for corrosion rates higher than 1% (right) and for the three loading speeds used. It can be seen: i) The deformation is similar for low and medium speeds regardless of the corrosion rate and ii) At high corrosion rates the deformation is much larger for the high loading speed.

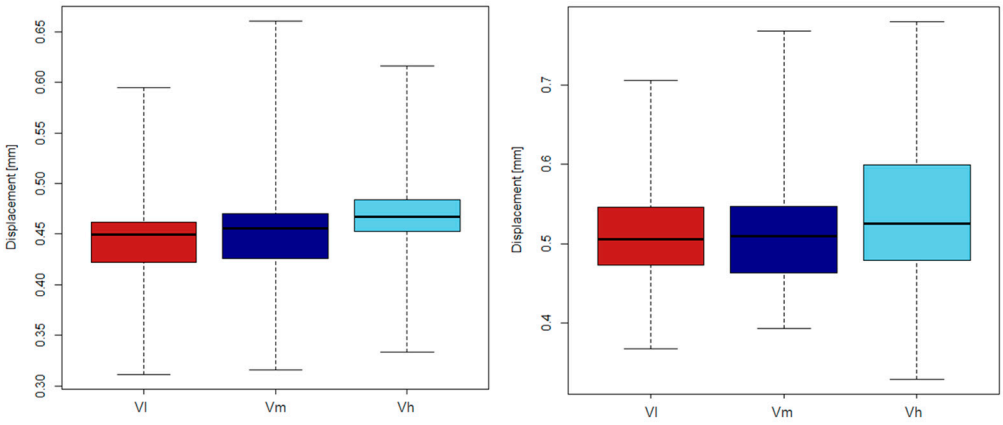

Figure 8. Deformation of bar specimens in the yield zone for corrosion rates under 1% (left) and over 1% (right) and for the three loading speeds Vl, Vm and Vh.

The evolution of the mechanical properties obtained in the tensile tests as a function of the corrosion rate is plotted in Figures 9, 10 and 11. Colours allow distinction of the loading speed.

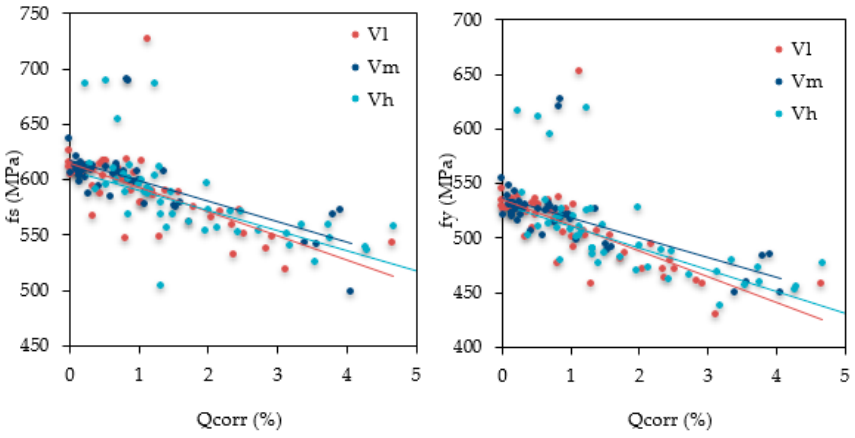

Figure 9. Effects of the corrosion rate and the loading speed on the tensile strength *fs* (left) and the elastic limit *fy* (right).

Preprints (www.preprints.org) | NOT PEER-REVIEWED | Posted: 28 January 2019 doi:10.20944/preprints201901.0279.v1

Peer-reviewed version available at Materials 2019, 12, 965; doi:10.3390/ma12060965

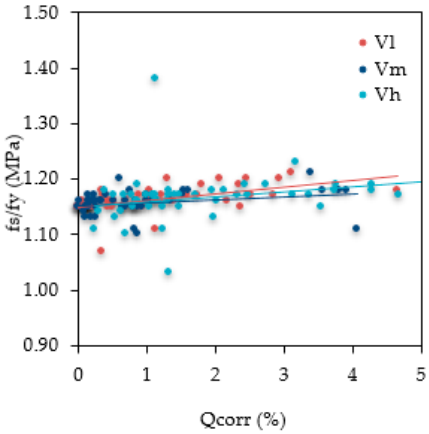

Figure 10. Effects of the corrosion rate and the loading speed on the ratio *fs*/*fy*.

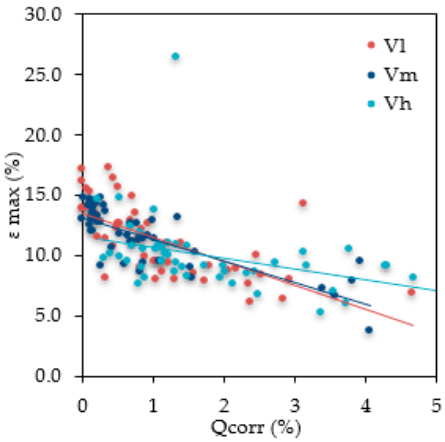

Figure 11. Effects of the corrosion rate and the loading speed on the strain at maximum load ε_{max}.

The values of the tensile strength *fs* and the elastic limit *fy* of Figure 9 have been obtained by dividing the acting load by the average cross section area of the specimen S_{res} after the corrosion process. If the corrosion would have been uniform along the bar the adjusting trend lines should have been horizontal. However, the lines are decreasing for all loading speeds. This is due to the fact that the corrosion is not homogeneous in the bar surface but occurs in series of pitting spots typical for chloride corrosion of steel. In these spots the cross section area of the bar is smaller than the average S_{res} control the test results. Additionally, the corrosion takes place in the outer thickness of the bar surface composed by martensite, a metallographic material produced by the rolling mill when the bar was fabricated. Martensite has higher strength properties (*fs*, *fy*) than the ferrite composing the internal core of the bar. The destruction of part of this stronger outer layer explains the reduction of the average strength values in the bar cross section.

Figure 12. Microscopy image of the corroded surface (left) of bar specimen B087M with Q_{corr} = 1.07% and the cross section (right).

Peer-reviewed version available at Materials 2019, 12, 965; doi:10.3390/ma12060965

The evolution of ratio *fs*/*fy* for the three loading speeds is shown in Figure 10. A slight increment of this ratio is observed, regardless of the loading speed. Again, this can be explained by the fact that the outer martensite presents higher values of *fs*/*fy* than the one of the ferrite in the bar core. When part of the martensite disappears the proportion of ferrite in the bar cross section increases and the ratio *fs*/*fy* becomes higher. Other reports with corrosion rates higher than the ones of this work show that the increments of ratio *fs*/*fy* are higher than the ones here reported [28].

Figure 13 shows the evolution of the three ductility parameters based on the steel equivalent concept as a function of the corrosion rate for the three loading speeds. All parameter values decrease when the corrosion rate increases regardless of the loading speed. Parameters *p* and *A** evolve similarly for low and medium loading speeds (parallel lines).

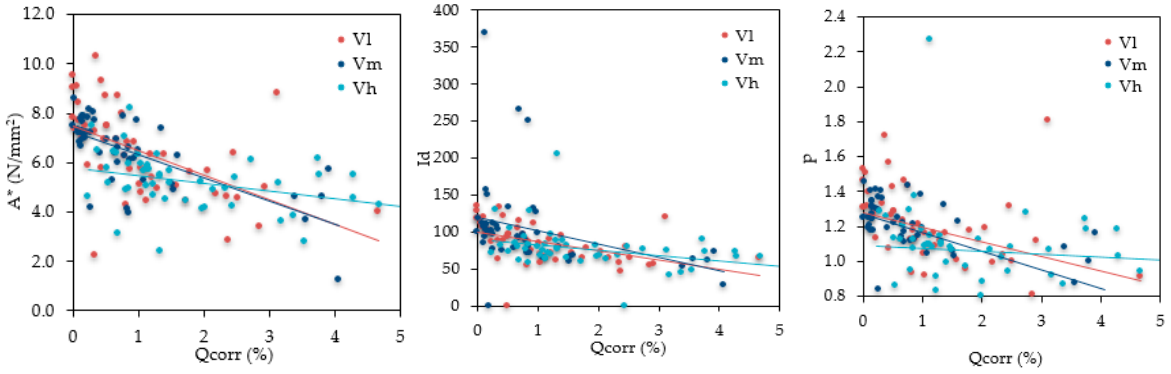

Figure 13. Effect of corrosion rate and loading speed on the equivalent steel concept parameters *A**, *Id* and *p*.

5. Conclusions

1) With the exception of the ratio *fs*/*fy* there is a systematic reduction of all strength and durability parameters (*fs*,*fy*, ε_{max}, *p*, *A** and *Id*) for increasing corrosion rates.

2) The increasing of the corrosion level leads to modifying the stress-strain diagram, losing the yield plateau and showing like cold-drawn behavior.

3) The loadinand showing g speed of the tensile test is a variable that, along with the corrosion rate, governs the values and the evolution of all of the studied parameters (except the ratio *fs*/*fy*).

4) The concept of equivalent steel is useful to evaluate the ductility behavior of corroded reinforcement bars in concrete. regardless of the loading speed in the tensile test.

5) The higher the tensile test loading speed, the higher is the yield zone in the strain-stress relationship curve.

6) With corrosion rates as low as 1% there is a change in the strain-stress curve so that in some cases the yield plateau disappears and the steel behaves as a cold-formed steel. 6. Patents

This section is not mandatory but may be added if there are patents resulting from the work reported in this manuscript.

Author Contributions: "conceptualization, A.M.B. and M.N.G; methodology, A.M.B. and M.N.G.; formal analysis, A.M.B. and M.N.G; investigation, A.M.B.; resources, A.M.B.; data curation, A.M.B and M.G.A.; writing—original draft preparation, A.M.B and M.G.A; writing—review and editing, M.G.A and J.C.G.; supervision, J.C.G.; project administration, J.C.G.; funding acquisition, A.M.B and J.C.G."

Funding: This research was funded by Spanish Ministry of Economy, Industry and Competitiveness, gran number BIA 2016 78742-C2-2-R. Also, this research was supported by an FPU contract-fellowship by the Spanish Ministry of Science and Innovation to Angela Moreno Bazan, grant number FPU14-06362.

Conflicts of Interest: The authors declare no conflict of interest.

References

1. EHE-08. Spanish Structural Concrete Code EHE-08. Spanish Minister of Public Works. (2008).

2. British Standards Institution. Eurocode 2: Design of Concrete Structures: Part 1-1: General Rules and Rules for Buildings. British Standards Institution (2004).
3. Rodríguez. J., L. M. Ortega. and J. Casal. "Load carrying capacity of concrete structures with corroded reinforcement." Construction and building materials11.4 (1997): 239-248.
4. Cairns, John. et al. "Mechanical properties of corrosion-damaged reinforcement." ACI Materials Journal 102.4 (2005): 256-264.
5. Zhang, Weiping, et al. "Tensile and fatigue behavior of corroded rebars." Construction and Building Materials 34 (2012): 409-417.
6. Apostolopoulos, Ch Alk. "Mechanical behavior of corroded reinforcing steel bars S500s tempcore under low cycle fatigue." Construction and Building Materials 21.7 (2007): 1447-1456.
7. Apostolopoulos, C. A., and V. G. Papadakis. "Consequences of steel corrosion on the ductility properties of reinforcement bar." Construction and Building Materials 22.12 (2008): 2316-2324.
8. Du. Y. G., L. A. Clark, and A. H. C. Chan, "Residual capacity of corroded reinforcing bars." Magazine of Concrete Research 57.3 (2005): 135-147.
9. Zhang W, Song X. Gu X, Li S. Tensile and fatigue behavior of corroded rebars. Construction and Building Materials 2012; 34: 409–17.
10. Cairns, John, et al. "Mechanical properties of corrosion-damaged reinforcement." ACI Materials Journal 102.4 (2005): 256-264.
11. UNE 36065: 2011, "Ribbed bars of weldable steel with special characteristics of ductility for the reinforcement of concrete. AENOR. 2011.
12. Maslehuddin, Mohammed, et al. "Effect of rusting of reinforcing steel on its mechanical properties and bond with concrete." ACI Materials Journal 87.5 (1990): 496-502.
13. Fernández, Ignasi, Jesús Miguel Bairán, and Antonio R. Marí, "Corrosion effects on the mechanical properties of reinforcing steel bars. Fatigue and σ–ε behavior." Construction and Building Materials 101 (2015): 772-783.
14. Cobo. A., E. Moreno, and M. F. Canovas, "Mechanical properties variation of B500SD high ductility reinforcement regarding its corrosion degree." Materiales de Construccion 61.304 (2011): 517-532.
15. Wang, Xiao-gang, et al. "Determination of residual cross-sectional areas of corroded bars in reinforced concrete structures using easy-to-measure variables." Construction and Building Materials 38 (2013): 846-853.
16. Saifullah. M., and L. A. Clark, "Effect of corrosion rate on the bond strength of corroded reinforcement." Proceedings of International Conference on Corrosion and Corrosion Protection of Steel in Concrete. Vol. 1. 1994.
17. Bazán. A. M., A. Cobo, and J. Montero, "Study of mechanical properties of corroded steels embedded concrete with the modified surface length." Construction and Building Materials 117 (2016): 80-87.
18. Moreno Fernandez. E., A. Cobo Escamilla, and M. Fernández Cánovas, "Ductility of reinforcing steel with different degrees of corrosion and the 'equivalent steel' criterion." Materiales de Construcción 57.286 (2007): 5-18.
19. DU BETON-CEB-FIP. COMITE EUROINTERNATIONAL. "Durable concrete structures. Design guide." (1992).
20. Cosenza, Edoardo, Carlo Greco, and Gaetano Manfredi, "The concept of equivalent steel." CEB Bulletin d'information 218 (1993): 163-84.
21. Cosenza, Edoardo, Carlo Greco, and Gaetano Manfredi, "An equivalent steel index in the assessment of the ductility performances of the reinforcement." BULLETIN D INFORMATION-COMITE EUROINTERNATIONAL DU BETON242 (1998): 157-170.
22. Creazza, G., and S. Russo, "A new proposal for defining the ductility of concrete reinforcement steels by means of a single parameter." BULLETIN D INFORMATION-COMITE EUROINTERNATIONAL DU BETON 242 (1998): 171-182.
23. Ortega. H, Estudio experimental de la influencia del tipo de acero en la capacidad de redistribución en losas de hormigón armado. Diss. PhD Thesis. Polytechnic University of Madrid. Madrid. 1998.
24. Real Decreto 256/2008. de 10 de junio Instrucción para la recepción de cementos (RC-16)
25. ASTM G1-03. "Standard practice for preparing. cleaning. and evaluating corrosion test specimens." (2003).
26. ISO 8407. "Corrosion of metals and alloys-Removal of corrosion products from corrosion test specimens." (1991).

27. UNE-EN ISO 15630-1:2011. Steel for the reinforcement and prestressing of concrete - test methods - part 1: reinforcing bars. wire rod and wire. AENOR 2011:28

28. Moreno, Esther, et al. "Mathematical models to predict the mechanical behaviour of reinforcements depending on their degree of corrosion and the diameter of the rebars." Construction and Building Materials 61 (2014): 156-163.